Cardiac SPECT radiomic features repeatability and reproducibility: A multi-scanner phantom study

Mohammad Edalat-Javid, MSc,[a] Isaac Shiri, MSc,[b] Ghasem Hajianfar, MSc,[c] Hamid Abdollahi, PhD,[d] Hossein Arabi, PhD,[b] Niki Oveisi, MSc,[e] Mohammad Javadian, PhD,[f] Mojtaba Shamsaei Zafarghandi, PhD,[a] Hadi Malek, MD,[c] Ahmad Bitarafan-Rajabi, PhD,[c,g,h] Mehrdad Oveisi, PhD,[c,i] and Habib Zaidi, PhD[b,j,k,l]

[a] Department of Energy Engineering and Physics, Amir Kabir University of Technology, Tehran, Iran
[b] Division of Nuclear Medicine and Molecular Imaging, Geneva University Hospital, Geneva 4, Switzerland
[c] Rajaie Cardiovascular Medical and Research Center, Iran University of Medical Science, Tehran, Iran
[d] Department of Radiologic Sciences and Medical Physics, Faculty of Allied Medicine, Kerman University, Kerman, Iran
[e] School of Population and Public Health, The University of British Columbia, Vancouver, BC, Canada
[f] Department of Computer Engineering, Faculty of Information Technology, Kermanshah University of Technology, Kermanshah, Iran
[g] Cardiovascular Intervention Research Center, Rajaie Cardiovascular Medical and Research Center, Iran University of Medical Sciences, Tehran, Iran
[h] Echocardiography Research Center, Rajaie Cardiovascular Medical and Research Center, Iran University of Medical Sciences, Tehran, Iran
[i] Department of Computer Science, University of British Columbia, Vancouver, BC, Canada
[j] Geneva University Neurocenter, Geneva University, Geneva, Switzerland
[k] Department of Nuclear Medicine and Molecular Imaging, University of Groningen, University Medical Center Groningen, Groningen, The Netherlands
[l] Department of Nuclear Medicine, University of Southern Denmark, Odense, Denmark

Received Nov 18, 2019; accepted Mar 12, 2020
doi:10.1007/s12350-020-02109-0

Background. **The aim of this work was to assess the robustness of cardiac SPECT radiomic features against changes in imaging settings, including acquisition, and reconstruction parameters.**

Methods. **Four commercial SPECT and SPECT/CT cameras were used to acquire images of a static cardiac phantom mimicking typical myorcardial perfusion imaging using 185 MBq of ^{99m}Tc. The effects of different image acquisition and reconstruction parameters, including**

Electronic supplementary material The online version of this article (https://doi.org/10.1007/s12350-020-02109-0) contains supplementary material, which is available to authorized users.

The authors of this article have provided a PowerPoint file, available for download at SpringerLink, which summarizes the contents of the paper and is free for re-use at meetings and presentations. Search for the article DOI on SpringerLink.com.''

Mohammad Edalat-Javid and Isaac Shiri have contributed equally to this manuscript

Reprint requests: Habib Zaidi, PhD, Geneva University Neurocenter, Geneva University, 1205 Geneva, Switzerland; *habib.zaidi@hcuge.ch*

1071-3581/$34.00

number of views, view matrix size, attenuation correction, as well as image reconstruction related parameters (algorithm, number of iterations, number of subsets, type of post-reconstruction filter, and its associated parameters, including filter order and cut-off frequency) were studied. In total, 5,063 transverse views were reconstructed by varying the aforementioned factors. Eighty-seven radiomic features including first-, second-, and high-order textures were extracted from these images. To assess reproducibility and repeatability, the coefficient of variation (COV), as a widely adopted metric, was measured for each of the radiomic features over the different imaging settings.

Results. **The Inverse Difference Moment Normalized (IDMN) and Inverse Difference Normalized (IDN) features from the Gray Level Co-occurrence Matrix (GLCM), Run Percentage (RP) from the Gray Level Co-occurrence Matrix (GLRLM), Zone Entropy (ZE) from the Gray Level Size Zone Matrix (GLSZM), and Dependence Entropy (DE) from the Gray Level Dependence Matrix (GLDM) feature sets were the only features that exhibited high reproducibility (COV ≤ 5%) against changes in all imaging settings. In addition, Large Area Low Gray Level Emphasis (LALGLE), Small Area Low Gray Level Emphasis (SALGLE) and Low Gray Level Zone Emphasis (LGLZE) from GLSZM, and Small Dependence Low Gray Level Emphasis (SDLGLE) from GLDM feature sets turned out to be less reproducible (COV > 20%) against changes in imaging settings. The GLRLM (31.88%) and GLDM feature set (54.2%) had the highest (COV < 5%) and lowest (COV > 20%) number of the reproducible features, respectively. Matrix size had the largest impact on feature variability as most of the features were not repeatable when matrix size was modified with 82.8% of them having a COV > 20%.**

Conclusion. **The repeatability and reproducibility of SPECT/CT cardiac radiomic features under different imaging settings is feature-dependent. Different image acquisition and reconstruction protocols have variable effects on radiomic features. The radiomic features exhibiting low COV are potential candidates for future clinical studies. (J Nucl Cardiol 2021;28:2730–44.)**

Key Words: SPECT/CT • radiomics • cardiovascular imaging • repeatability • reproducibility

Abbreviations

SPECT	Single-photon emission computed tomography
COV	Coefficient of variation
GLCM	Gray level co-occurrence matrix
GLRLM	Gray level co-occurrence matrix
GLSZM	Gray level size zone matrix
GLDM	Gray level dependence matrix
IDMN	Inverse difference moment normalized
LALGLE	Large area low gray level emphasis
SALGLE	Small area low gray level emphasis
SDLGLE	Small dependence low gray level emphasis

INTRODUCTION

As one of the major causes of mortality worldwide, cardiovascular disease is among the main concerns in public health.[1] Myocardial perfusion imaging (MPI) is a valuable non-invasive clinical tool enabling the functional assessment of coronary artery disease (CAD) to identify patients at risk with the aim to improve patient management.[2] In this regards, molecular imaging modalities, including single-photon emission computed tomography (SPECT) and positron emission tomography (PET), remain the most common procedures for the evaluation and risk stratification of patients with known or suspected CAD.[3] Previous studies indicated that SPECT and SPECT/CT provide high image quality, low radiation exposure, and high diagnostic accuracy for the management of CAD.[4,5] Advances in nuclear cardiac imaging instrumentation and clinically validated software, including novel resolution recovery reconstruction algorithms incorporating correction for detector response, have enhanced image quality and quantitative accuracy in nuclear cardiovascular imaging.[6,7]

Recently, quantitative radiomic studies have opened new horizons for better management of a number of diseases, including cancer and CAD.[8-12] The aim of radiomics is to extract quantitative features from medical images using data-mining algorithms for survival, prognosis, and therapeutic response prediction and assessment.[8,13] In this context, radiomics could provide valuable information for personalized medicine. Previous studies have suggested that radiomic features could act as biomarkers to characterize and predict disease to provide support for patient management.[8,14]

Radiomics have been widely used for the detection, diagnosis and prognosis of a number of diseases, including brain disorders,[15,16] various cancer types,[8,17] and more recently in cardiac diseases[18-21] using MRI, CT, and PET imaging modalities. With respect to the use of SPECT radiomics, this imaging modality has not been exploited to its full potential owing to its low spatial resolution and sensitivity. However, a number of recent studies demonstrated promising results using SPECT radiomic analysis in brain[15,16] and cardiac[18,19,22,23] disease management.

Medical image analysis remains a human enterprise. Owing to limitations of the human eyes and medical monitor display systems, a substantial amount of imperceptible but feature-rich information is unwittingly discarded.[24] To address this issue, radiomics quantifies medical images through mathematical extraction of different feature sets, thus enabling potential retrieval of the hidden information.

Based on biomarker discovery guidelines and studies, repeatability and reproducibility assessment of biomarkers are essential ingredients prior to clinical decision-making.[25] Regarding repeatability and reproducibility assessment, a reliable radiomic feature remains stable between two measurements when certain conditions change. Ideally, the features should also remain the same while the experimental settings, including equipment, software, processor, or operator vary.[26] When these conditions are fulfilled, the feature may be considered as a good biomarker for clinical setting. Hence, a considerable amount of literature has been published on radiomic features repeatability and reproducibility against changes in the radiomics generation process, such as image acquisition, reconstruction, pre-processing, segmentation, and data analysis.[27-29] Nuclear radiomic studies have tested the repeatability and reproducibility of imaging features over various imaging parameters including reconstruction algorithms, matrix size, iteration number, number of subsets, and post-filtering using both phantom and clinical studies.[26,29,30] To overcome such vulnerability, it was suggested to consider the reproducibility and repeatability of radiomic features as a feasible measure to preselect features for further analysis[8] These analyses (repeatability and reproducibility) are main frontiers, critical, and important tests in image biomarkers development to find robust features as imaging biomarkers based on the recommendations of the Quantitative Imaging Biomarker Alliance (QIBA) Technical Performance Working Group.[31]

To date, little evidence has been reported on cardiac SPECT imaging repeatability and reproducibility over different imaging settings. The present study aims to assess the repeatability and reproducibility of radiomic features using a dedicated cardiac phantom against variations in image acquisition and reconstruction protocols.

MATERIALS AND METHODS

Figure 1 illustrates the framework followed in this study. Additional details are given in the following section.

Data Acquisition

SPECT scans of a static cardiac phantom mimicking myocardial perfusion studies with and without defect inserts were performed on three commercial dual-headed SPECT/CT systems, including the GE Infinia HAWKEYE (GE Healthcare), Symbia T2 and Symbia T6 (Siemens Healthcare), as well as the BrightView dual-headed SPECT camera (Philips Healthcare). Representative images SPECT images of the cardiac phantom study showing typical image quality acquired on the four cameras with and without the defect are shown in Figure 2. A commercially available static phantom mimicking the shape of a normal heart within the thorax was used in these experiments (Data Spectrum Corporation, Inc.). The left ventricular myocardial wall was filled with water solution mixed with 185 MBq of ^{99m}Tc to avoid any saturation-related loss of count-rate. This phantom was placed within the cylindrical Jaszczak phantom and was surrounded by water. To mimic a realistic position of the myocardium in the chest, the Jaszczak phantom was placed in the center of the field-of-view and oriented in the 45 left-anterior and 45 caudal directions. The time per projection was set to 25 seconds per projection. Three defects were also added to simulate typical clinical abnormalities. Data acquisitions were performed on the four cameras equipped with a low energy high resolution collimator (LEHR) using different acquisition parameters, such as number of views, view matrix size, with or without attenuation correction.

Image Reconstruction

To study the impact of reconstruction settings on image/radiomic features, six different image reconstruction methods were used, including filtered backprojection (FBP), maximum likelihood-expectation maximization (MLEM), ordered subset-expectation maximization (OSEM), WALLIS MLEM software package (Siemens Healthcare), FLASH 3D depth-dependent 3D OSEM reconstruction (Siemens Healthcare), resolution recovery ASTONISH reconstruction (Philips Healthcare). The effects of different reconstruction settings, including the number of iterations, number of subsets, post-reconstruction filters (Butterworth, Hanning, Metz, Shepp Logan, Gaussian, Parzan) and their associated parameters, such as full-width at half-maximum (FWHM) (for the Gaussian filter), filter-order and cut-off frequency (for the Butterworth filter) were considered for the four cameras, whereas CT-based attenuation correction was considered only for the 3 SPECT/CT systems.

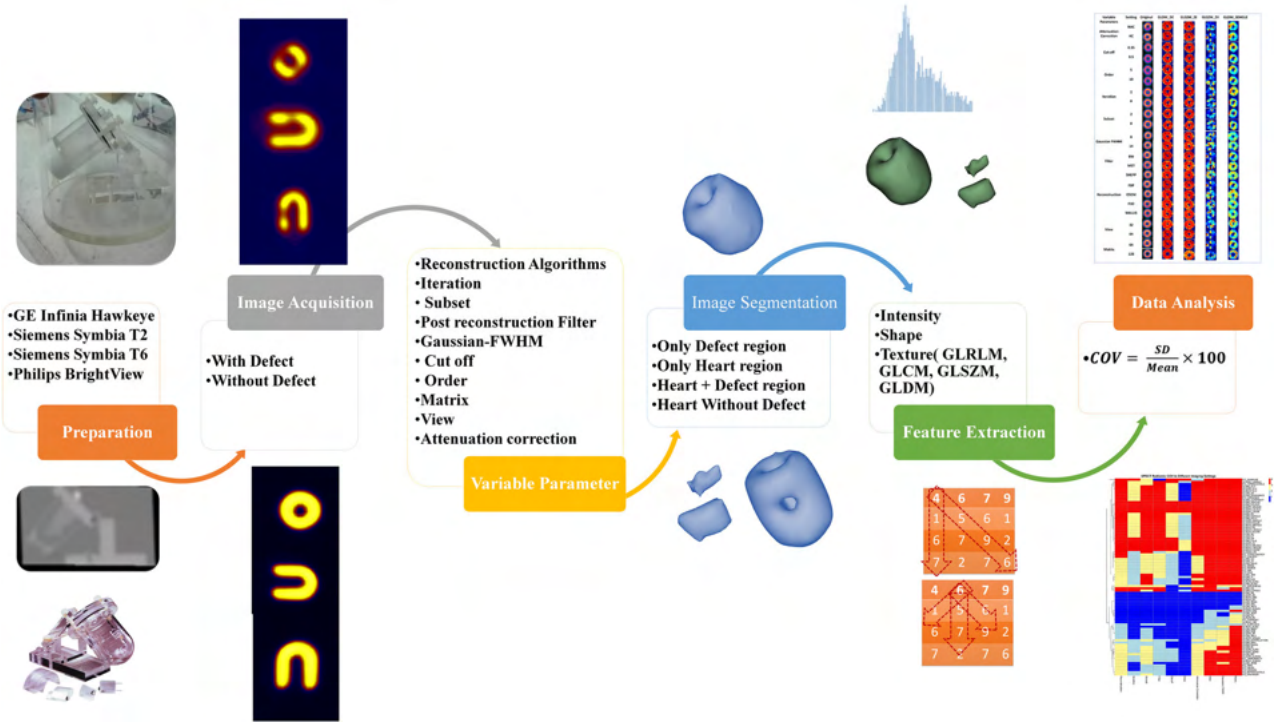

Figure 1. Representative SPECT images of the cardiac phantom study showing typical image quality produced on (from left to right): Philips BrightView SPECT camera, Siemens Symbia T2, Siemens Symbia T6 and GE Infinia Hawkeye SPECT/CT cameras and (from top to bottom): Short-axis, vertical and horizontal long axis without (first row) and with the defect (second row). The reconstruction parameters are as follows: FBP reconstruction, 64 × 64 matrix size, 32 views, 5th order Butterworth post-reconstruction filter with 0.5 cut-off frequency).

Table 1 presents the detailed list of settings/parameters used for the reconstruction of the cardiac phantom.

To minimize the pixel size effect, we calculated the FOV and zoom factor using the following equation to get the same pixel size for all studies.

$$\text{Pixel size} = \frac{\text{FOV}}{\text{Zoom factor} \times \text{Matrix size}}$$

Overall, 5,063 tomographic image reconstructions were performed considering virtually all possible combinations/variations of reconstruction settings/parameters. Supplemental Figures 1 to 9 illustrate normal and perfusion defective SPECT cardiac images of the phantom in different views acquired on various cameras.

Image Segmentation

All image segmentations were performed manually using the 3D-Slicer software on short axis slices. The latter is an open-source software used for medical image analysis, including segmentation, registration, and visualization.[32] For the cardiac phantom without defects, the whole myocardium was segmented, whereas for scans acquired with defects three regions were delineated including the defect region, whole myocardium, and whole myocardium minus the defect region. To minimize the impact of image segmentation on the results, a single VOI was defined and copied on all reconstructions.

Feature Extraction

Eighty-seven radiomic features, including first order statistics (FOS, n=18), and first-, second- and high-order texture features were extracted from the 5,063 reconstructed phantom images. Image feature extraction was performed using the PyRadiomics Python library,[33] an open source package developed according to consensus definitions of the Image biomarker standardization initiative (IBSI).[26] The feature set consisted of second-order texture features, including Gray Level Co-occurrence Matrix (GLCM, n = 23), and high-order texture features, including Gray Level Run Length Matrix (GLRLM, n = 16), Gray Level Dependence Matrix (GLDM, n = 14), and Gray Level Size Zone Matrix (GLSZM, n = 16). FOS features calculate only the intensity values without considering the relationship between pixels, such as the mean and maximum of intensity in a volume of interest. In second-order texture features (such as the GLCM), in addition to the intensity, the repetition of similar intensities occuring next to each other would be considered (relationship between two voxels). In high-order texture features, the relationship of three or more voxels would be calculated. Table 2 summarizes

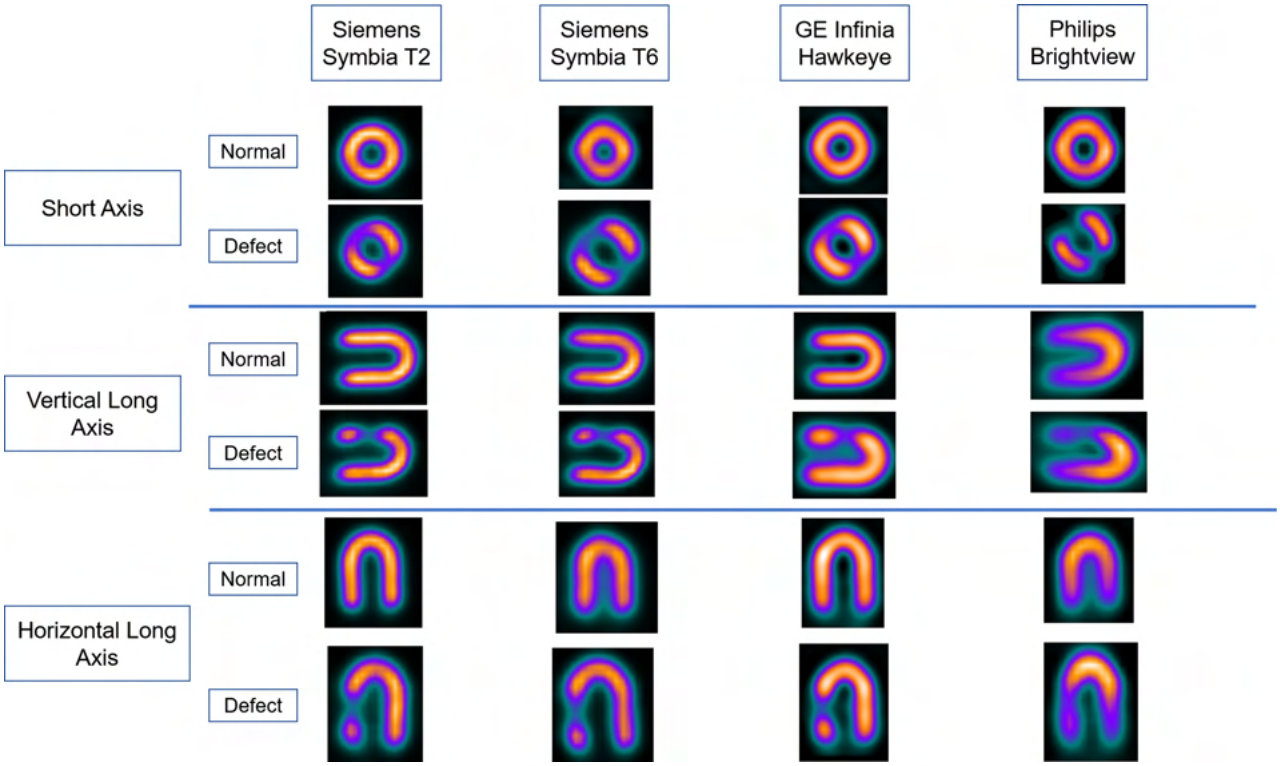

Figure 2. Flowchart of the radiomics framework employed in the present work.

all radiomic features considered in this work, whereas Supplemental Tables 1 to 5 provide additional details about their mathematical formulation.

Statistical Analysis

To assess the reproducibility and repeatability of the extracted radiomic features, the coefficient of variation (COV) was calculated for each feature across all reconstructed images using Eq. (1).

$$\mathrm{COV} = \frac{\mathrm{SD}}{\mathrm{Mean}} \times 100 \qquad (1)$$

where SD and Mean stand for the standard deviation and average of a feature quantity across all reconstructions. Given the COV values for different features, four reproducibility categories were defined based on which the radiomic features were ranked[30,34]: very small (COV $\leq$ 5%), small (5% $<$ COV $\leq$ 10%), intermediate (10% $<$ COV $\leq$ 20%) and large (COV $>$ 20%).

RESULTS

Figure 3 depicts the heat map of radiomic features categorized based on COV (1: very small (COV $\leq$ 5%), 2: small (5% $<$ COV $\leq$ 10%), 3: intermediate (10% $<$ COV $\leq$ 20%) and 4: large (COV $>$ 20%). For different image reconstruction and acquisition settings, the DE from GLDM, ZE and RLNUN and SRE and RP from GLRLM, IDMN and IDN, IMC2 from GLCM features were the most (COV $\leq$ 5%) reproducible features. The SDLGLE, LDLGLE and DV from GLDM, and SALGLE, LALGLE and LGLZE from GLSZM were less reproducible (COV $>$ 20%), with respect to all reconstruction and acquisition settings. Figure 4 shows an example of high and low reproducible features in different imaging settings. It can be observed that the feature map of reproducible features (DE from GLDM and ZE from GLSZM) didn't change under different image settings. The variability of non-reproducible features (ZV from GLSZM and SDHGLE from GLDM) can be seen in different settings. Figure 5 depicts the percentage of different COV categories for each feature in all imaging settings (Supplemental Table 7).

Figure 6a presents the percentage of different COV groups for feature sets (details presented in Supplemental Table 6). The GLRLM (31.88%) and GLCM (30.43%) feature sets had the highest number of reproducible features, whereas the GLDM feature set (54.2%) had the lowest number of reproducible feature sets. Figure 6b depicts the percentage of different COV groups for various imaging settings (details presented in Table 3). The matrix size, number of views and the

Table 1. List of variable and invariable image acquisition and reconstruction parameters

Parameter studied	Variable	Constant
Reconstruction algorithm	FBP, OSEM, FLASH 3D, ASTONISH, MLEM, WALLIS	Iterations = 2, Subsets = 8, Filter = BW, Cutoff = 0.5, Order = 10, Matrix = 64, Views = 64
Iterations	2, 4, 6, 8, 10, 12, 14, 16	FWHM = 5 mm, Views = 32, Matrix = 64, Subset = 8
Subsets	2, 6, 4, 8	Iterations = 2, FWHM = 5 mm Matrix = 64, Views = 32
Filter type	Butterwort, Hanning, Metz, Shepp Logan, Gaussian, Parzan	Matrix = 64, Views = 64 cutoff = 0.5, Order = 10
Filter (FWHM mm) (Gaussian)	2, 2.5, 3, 3.5, 4, 4.5, 5, 5.5, 6, 6.5, 7, 8	Iteration = 2, Subset = 8 Matrix = 64, Views64
Cut-off frequency (Butterworth)	0.35, 0.4, 0.45, 0.5, .55	Matrix = 64, Views = 32 Filter = BW, Order = 10
Filter order (Butterworth)	1.5, 1.75, 2, 5, 9, 10,	Matrix = 64, Views = 32 Filter = BW, Cut off = 0.5
Attenuation correction	Device type	Matrix = 64, Views = 64, Filter = BW Cutoff = 0.5, Order = 10
Matrix size	64, 128	Views = 64, Filter = BW Cutoff = 0.5, Order = 5
Number of views	32, 64, 128	Matrix = 64, Filter = BW Cut off = 0.5, Order = 5

BW Butterworth filter

FWHM of the Gaussian filter led to 82.8%, 70.1% and 67.8%, respectively, of features having a COV $> 20\%$ (non-reproducible features). In addition, the filter order, cut-off frequency, and number of iterations led to 69%, 37.9%, and 28.7%, respectively, of features having a COV $< 5\%$, demonstrating a low variability. Supplemental Tables 8 to 17 summarize the results for each imaging setting.

DISCUSSION

Radiomics has emerged as a promising approach for effective disease management through non-invasive, fast, straightforward, and cost-effective quantitative image analysis.[14] In this approach, features extracted from medical images are used for clinical applications and disease management. However, it is important to note that radiomics-based analysis suffers from fluctuations in features quantification against changing imaging settings, segmentation, and processing.[25,35] Hence, previous studies have suggested that radiomic features must be assessed in terms of repeatability, reproducibility, and robustness before applying them in clinical decision-making.

This work analyzed the reproducibility of cardiac SPECT radiomics features against changes in imaging settings, including reconstruction algorithm, number of iterations and subsets, image matrix size, attenuation correction, number of views and different post-reconstruction filters and their associated parameters, such as FWHM of Gaussian filtering, cut-off frequency and filter order. The results showed that a number of features are reproducible while others are not. It was also found that the effects of different imaging settings are dependent on the type of setting and feature characteristics. As shown in the heat map, IDMN and IDN features from GLCM, RP from GLRLM, ZE from GLSZM, and DE from the GLDM feature sets were the only features that were highly reproducible (COV $\leq 5\%$) against all changes in imaging settings. In addition, LALGLE, SALGLE, and LGLZE features from GLSZM and SDLGLE feature from GLDM feature sets were the only features that were less reproducible (COV $> 20\ \%$)

Table 2. List of adopted radiomic features

First order statistics (FOS)	Gray level co-occurrence matrix (GLCM)	Gray level run length matrix (GLRLM)
1. Energy	1. Autocorrelation (AC)	1. Short Run Emphasis (SRE)
2. Total Energy	2. Joint Average (JA)	2. Long Run Emphasis (LRE)
3. Entropy	3. Cluster Prominence (CP)	3. Gray Level Non-Uniformity (GLN)
4. Minimum	4. Cluster Shade (CS)	4. Gray Level Non-Uniformity Normalized (GLNN)
5. 10th percentile	5. Cluster Tendency (CT)	5. Run Length Non-Uniformity (RLN)
6. 90th percentile	6. Contrast	6. Run Length Non-Uniformity Normalized (RLNN)
7. Maximum	7. Correlation	7. Run Percentage (RP)
8. Mean	8. Difference Average (DAve)	8. Gray Level Variance (GLV)
9. Median	9. Difference Entropy (DEnt)	9. Run Variance (RV)
10. Interquartile Range (IQR)	10. Difference Variance (DVariance)	10. Run Entropy (RE)
11. Range	11. Joint Energy (JEne)	11. Low Gray Level Run Emphasis (LGLRE)
12. Mean Absolute Deviation (MAD)	12. Joint Entropy (JEnt)	12. High Gray Level Run Emphasis (HGLRE)
13. Robust Mean Absolute Deviation (RMAD)	13. Informal Measure of Correlation (IMC) 1	13. Short Run Low Gray Level Emphasis (SRLGLE)
14. Root Mean Squared (RMS)	14. Informal Measure of Correlation (IMC) 2	14. Short Run High Gray Level Emphasis (SRHGLE)
15. Skewness	15. Inverse Difference Moment (IDM)	15. Long Run Low Gray Level Emphasis (LRLGLE)
16. Kurtosis	16. Inverse Difference Moment Normalized (IDMN)	16. Long Run High Gray Level Emphasis (LRHGLE)
17. Variance	17. Inverse Difference (ID)	
18. Uniformity	18. Inverse Difference Normalized (IDN)	
	19. Inverse Variance (IV)	
	20. Maximum Probability (MP)	
	21. Sum Average (SA)	
	22. Sum Entropy (SE)	
	23. Sum of Squares (SS)	

Gray Level Size Zone Matrix (GLSZM)	Gray Level Dependence Matrix (GLDM)
1. Small Area Emphasis (SAE)	1. Small Dependence Emphasis (SDE)
2. Large Area Emphasis (LAE)	2. Large Dependence Emphasis (LDE)
3. Gray Level Non-Uniformity (GLN)	3. Gray Level Non-Uniformity (GLN)
4. Gray Level Non-Uniformity Normalized (GLNN)	4. Dependence Non-Uniformity (DN)
5. Size-Zone Non-Uniformity (SZN)	5. Dependence Non-Uniformity Normalized (DNN)
6. Size-Zone Non-Uniformity Normalized (SZNN)	6. Gray Level Variance (GLV)
7. Zone Percentage (ZP)	7. Dependence Variance (DV)
8. Gray Level Variance (GLV)	8. Dependence Entropy (DE)
9. Zone Variance (ZV)	9. Low Gray Level Emphasis (LGLE)
10. Zone Entropy (ZE)	10. High Gray Level Emphasis (HGLE)
11. Low Gray Level Zone Emphasis (LGLZE)	11. Small Dependence Low Gray Level Emphasis (SDLGLE)
12. High Gray Level Zone Emphasis (HGLZE)	12. Small Dependence High Gray Level Emphasis (SDHGLE)

Table 2 continued

Gray Level Size Zone Matrix (GLSZM)	Gray Level Dependence Matrix (GLDM)
13. Small Area Low Gray Level Emphasis (SALGLE)	13. Large Dependence Low Gray Level Emphasis (LDLGLE)
14. Small Area High Gray Level Emphasis (SAHGLE)	14. Large Dependence High Gray Level Emphasis (LDHGLE)
15. Large Area Low Gray Level Emphasis (LALGLE)	
16. Large Area High Gray Level Emphasis (LAHGLE)	

against changes in imaging settings. The results can be applied in clinical setting aiming to come-up with relevant imaging biomarkers.

The results showed that the matrix size had the greatest impact on feature variability, which is in agreement with previous studies focusing on PET/CT radiomic features.[30] After matrix size, the number of views had the largest impact on the fluctuation of radiomics feature values. Cardiac radiomics analysis, as a newly introduced approach, has recently attracted attention in the literature.

Radiomic studies have mostly focused on oncology, yet there is a small but steadily increasing number of studies reporting on cardiac disease assessment using features extracted from MRI and CT images[18-21] and more recently from SPECT images.[18,19,22,23] A study by Kolossváry et al.[20] showed that radiomic features are superior to conventional quantitative computed tomographic metrics in identifying coronary plaques with napkin-ring signs. Neisius et al.[21] examined the diagnostic capability of cardiovascular magnetic resonance image radiomic features in differentiating between hypertensive heart disease (HHD) and hypertrophic cardiomyopathy (HCM). Their study showed that native T1-weighted imaging discriminates between HHD and HCM patients and provides incremental value over global native T1-weighted mapping. Recently Kolossváry et al.[36] developed a radiomics-based machine learning method, which improves the identification of advanced atherosclerotic lesions from CT angiography images.

Ashrafinia et al.[18,19,22,23] applied clinical MPI SPECT features to predict coronary artery calcification (CAC). CAC scoring determined from CT scans is a highly specific marker for coronary atherosclerosis disease management.[37,38] Since routine MPI SPECT has limited value in detecting calcification and stenosis (do not result in abnormal MPI SPECT),[39,40] the above studies proposed a radiomics signature from MPI SPECT images for CAC score prediction. They reported significant correlation between perfusion heterogeneity and CAC scores, thus providing valuable information to potentially add diagnostic and prognostic value to MPI SPECT.

A wide range of studies have been conducted to look after the repeatability and reproducibility of radiomic features. Recently, Traverso et al.[27] analyzed which types of radiomic features have been shown to be repeatable/reproducible in the peer-reviewed literature, and the degree of repeatability and reproducibility that might be achievable. However, this review didn't cover existing research on SPECT radiomic features repeatability and reproducibility. To the best of our knowledge, the current study is the first work reporting on this topic and, as such, its outcome could be beneficial for researchers working in the field of cardiac SPECT radiomics.[18,19,22,23] As a main limitation of radiomics analysis to become first line in clinical decision-making is the variability of radiomic features over changes in image acquisition, reconstruction, and processing techniques.[25,30,41] To overcome this vulnerability, it is suggested to consider the reproducibility and repeatability of radiomic features as a potential measure to preselect features for further analysis [8] . The success of radiomic features in clinical setting depends on their robustness, which is the main aim of current study. As such, our results would be valuable for future MPI SPECT radiomics research aiming at discovering novel diagnostic and prognostic cardiac SPECT imaging tools.

Although these results are significant, this study bears some limitations. This study focused only on experimental phantom studies. Large-scale clinical cardiac studies are needed to complete the present work by properly exploring the impact of biological factors on

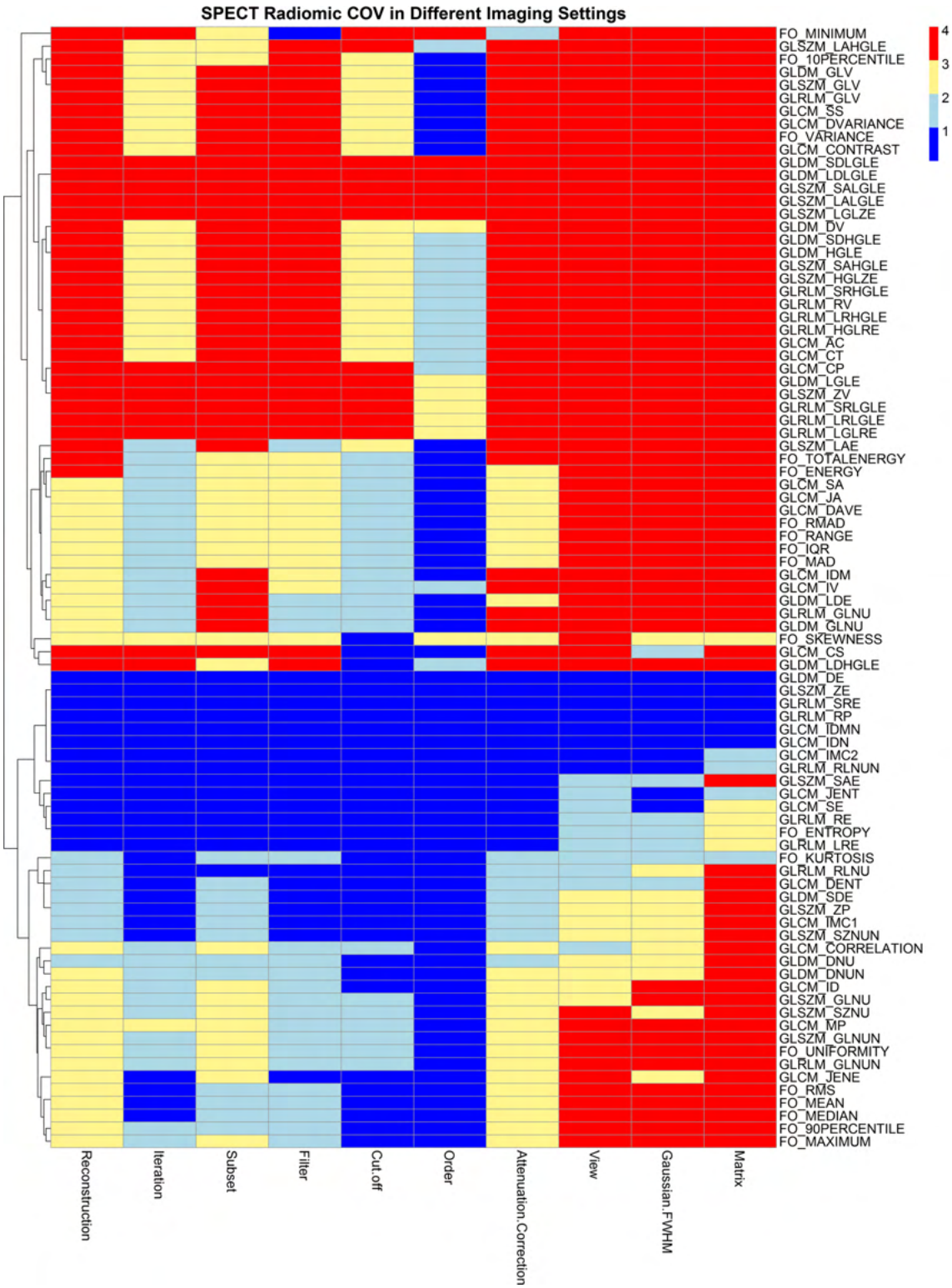

Figure 3. Heat map of SPECT radiomics COV for different imaging settings.

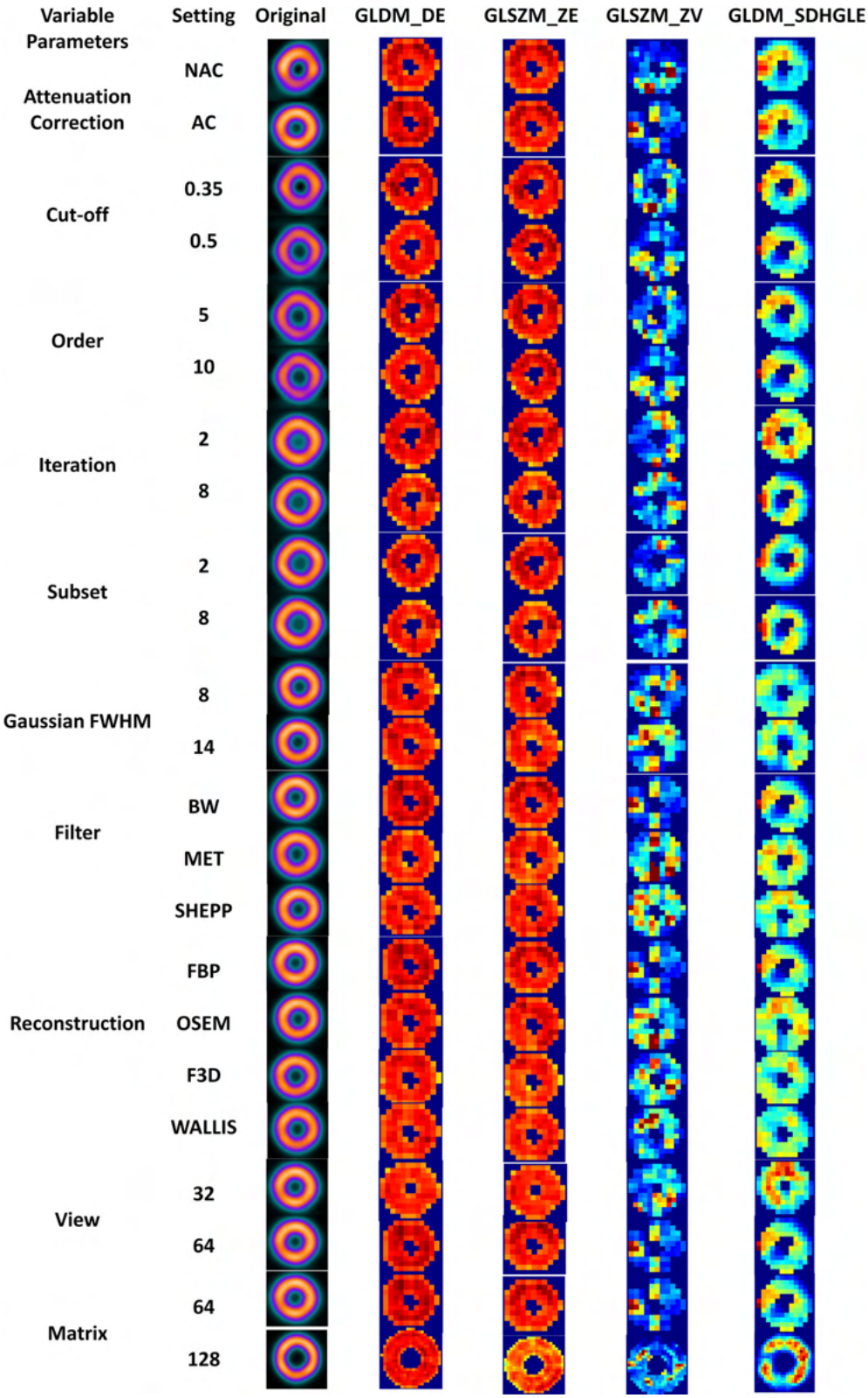

Figure 4. Example of high and low reproducible features in different imaging settings. *GLDM*, Gray level dependence matrix; *GLSZM*, gray level size zone matrix; *DE*, dependence entropy, *ZE*, zone entropy; *ZV*, zone variance; *SDHGLE*, small dependence high gray level emphasis.

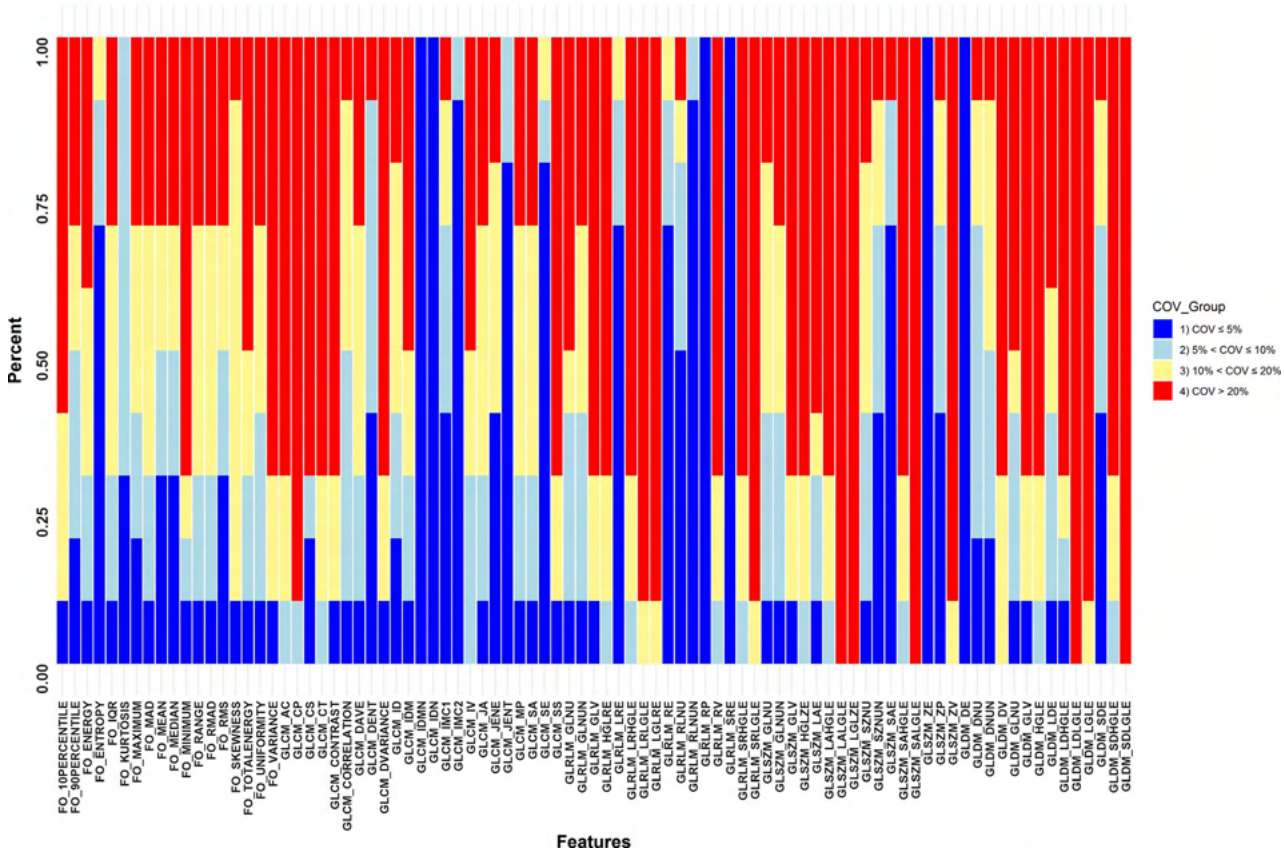

Figure 5. Bar plot of radiomic features for all image acquisition and reconstruction settings.

radiomic features. The phantom used in this work underestimates the magnitude of attenuation in MPI SPECT and its variation due to lungs, breasts, bones, …etc. In addition, there was no background or significant nearby concentration of extra-cardiac activity.

CONCLUSION

This multi-scanner cardiac phantom study investigated the reproducibility of cardiac SPECT radiomic features against changes in imaging settings, including reconstruction algorithms, number of iterations and subsets, matrix size, attenuation correction, number of views, post-reconstruction filters and their associated parameters. The repeatability and reproducibility of SPECT/CT radiomic features under different imaging

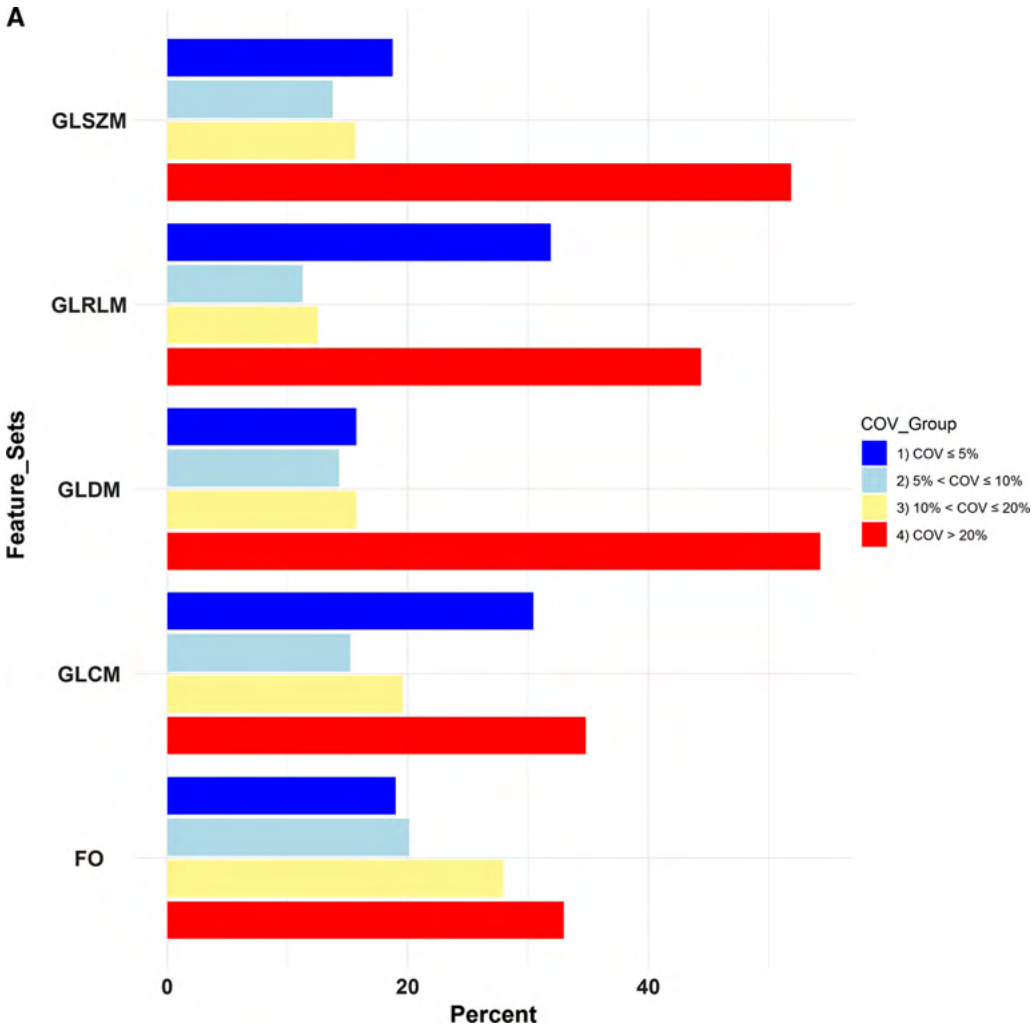

Figure 6. A Bar plot of COV groups for different feature sets in all image acquisition and reconstruction settings. **B** Bar plot of COV groups for different image acquisition and reconstruction settings. *FO*, First order; *GLCM*, gray level co-occurrence matrix; *GLRLM*, gray level run length matrix; *GLDM*, gray level dependence matrix; *GLSZM*, gray level size zone matrix.

settings is feature-dependent. In addition, different image acquisition and reconstruction protocols have variable effects on radiomic features. The radiomic features exhibiting low COV are potentially relevant candidates for future clinical studies.

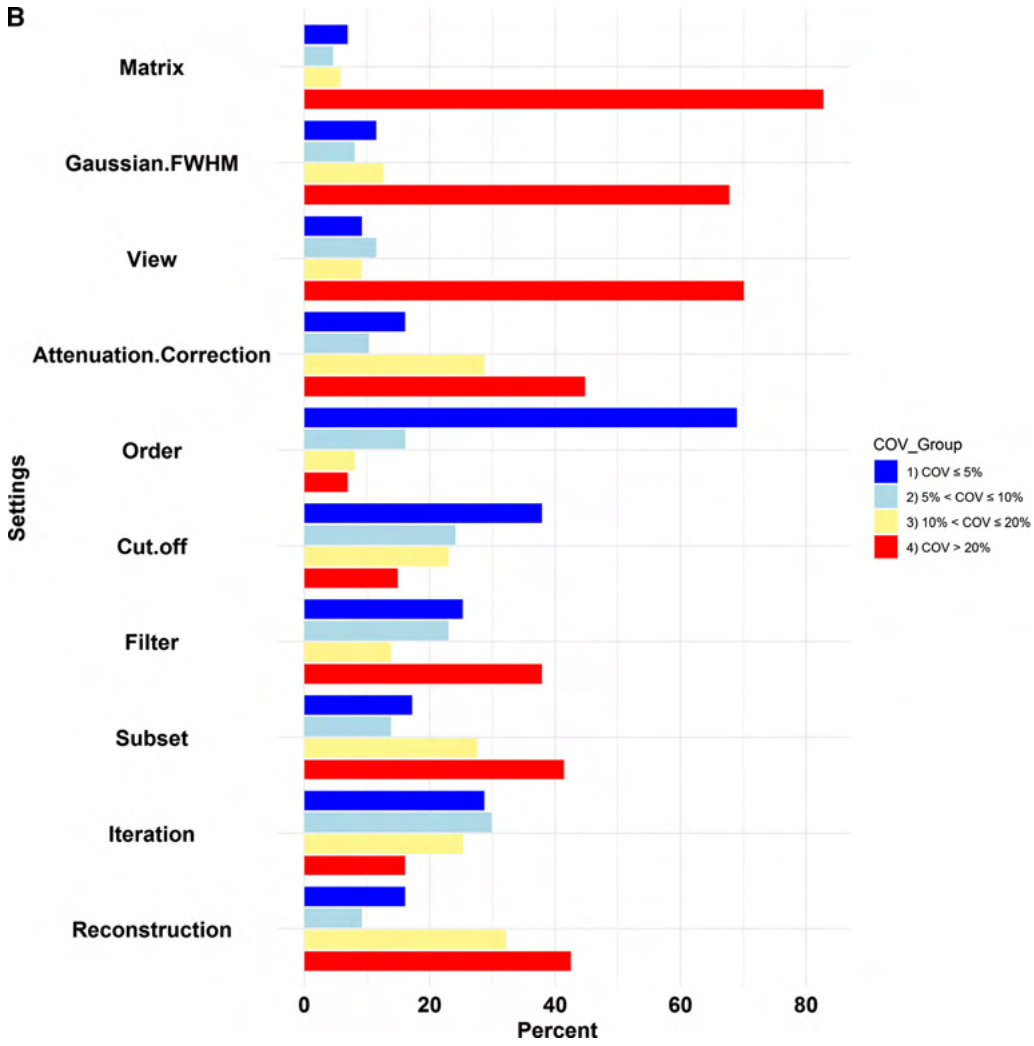

Figure 6. continued.

Table 3. The Percent of occurrence of different COV categories for different image reconstruction settings/parameters

Settings	COV ≤ 5%	5% < COV ≤ 10%	10% < COV ≤ 20%	COV > 20%
Reconstruction	16.1	9.2	32.2	42.5
Iteration	28.7	29.9	25.3	16.1
Subset	17.2	13.8	27.6	41.4
Filter	25.3	23	13.8	37.9
Cut off	37.9	24.1	23	14.9
Order	69	16.1	8.05	6.9
Attenuation correction	16.1	10.3	28.7	44.8
View	9.2	11.5	9.2	70.1
Gaussian FWHM	11.5	8.05	12.6	67.8
Matrix	6.9	4.6	5.75	82.8

NEW KNOWLEDGE GAINED

In the present work, we evaluated the reproducibility of cardiac radiomic features when using different image acquisition and reconstruction settings in a multi-scanner study using an experimental phantom. The results could be valuable for future SPECT-MPI radiomics-based research aiming at discovering novel diagnostic and prognostic cardiac SPECT imaging tools.

Acknowledgments

This work was supported by the Swiss National Science Foundation under grant SNFN 320030_176052.

Disclosure

Mohammad Edalat-Javid, Isaac Shiri, Ghasem Hajianfar, Hamid Abdollahi, Hossein Arabi, Niki Oveisi, Mohammad Javadian, Mojtaba Shamsaei Zafarghandi, Hadi Malek, Ahmad Bitarafan-Rajabi, Mehrdad Oveisi, and Habib Zaidi declare that they have no conflict of interest.

References

1. Bauer UE, Briss PA, Goodman RA, Bowman BA. Prevention of chronic disease in the 21st century: Elimination of the leading preventable causes of premature death and disability in the USA. Lancet 2014;384:45-52.
2. Greenland P, Alpert JS, Beller GA, Benjamin EJ, Budoff MJ, Fayad ZA, et al. 2010 ACCF/AHA guideline for assessment of cardiovascular risk in asymptomatic adults: A report of the American College of Cardiology Foundation/American Heart Association Task Force on Practice Guidelines. J Am Coll Cardiol 2010;56:e50-103.
3. Slomka P, Hung GU, Germano G, Berman DS. Novel SPECT technologies and approaches in cardiac imaging. Cardiovasc Innov Appl 2016;2:31-46.
4. Abdollahi H, Shiri I, Salimi Y, Sarebani M, Mehdinia R, Deevband MR, et al. Radiation dose in cardiac SPECT/CT: An estimation of SSDE and effective dose. Eur J Radiol 2016;85:2257-61.
5. Juan Ramon A, Yang Y, Wernick MN, Pretorius PH, Johnson KL, Slomka PJ, et al. Evaluation of the effect of reducing administered activity on assessment of function in cardiac gated SPECT. J Nucl Cardiol 2019. https://doi.org/10.1007/s12350-018-01505-x.
6. Zaidi H. Quantitative SPECT: Recent developments in detector response, attenuation and scatter correction techniques. Phys Med 1996;12:101-17.
7. Watson DD. Quantitative SPECT techniques. Semin Nucl Med 1999;29:192-203.
8. Lambin P, Leijenaar RTH, Deist TM, Peerlings J, de Jong EEC, van Timmeren J, et al. Radiomics: The bridge between medical imaging and personalized medicine. Nat Rev Clin Oncol 2017;14:749-62.
9. Abdollahi H, Mostafaei S, Cheraghi S, Shiri I, Rabi Mahdavi S, Kazemnejad A. Cochlea CT radiomics predicts chemoradiotherapy induced sensorineural hearing loss in head and neck cancer patients: A machine learning and multi-variable modelling study. Phys Med 2018;45:192-7.
10. Al-Mallah MH. Radiomics in hypertrophic cardiomyopathy: The new tool. JACC Cardiovascular imaging 2019;12:1955-7.
11. Kolossvary M, De Cecco CN, Feuchtner G, Maurovich-Horvat P. Advanced atherosclerosis imaging by CT: Radiomics, machine learning and deep learning. J Cardiovasc Comput Tomogr 2019;13(5):274-80.
12. Kolossváry M, Maurovich-Horvat P. Cardiac CT radiomics. In: Schoepf UJ, editor. CT of the Heart. Totowa, NJ: Humana Press; 2019. p. 715-24.
13. Reuze S, Schernberg A, Orlhac F, Sun R, Chargari C, Dercle L, et al. Radiomics in nuclear medicine applied to radiation therapy: Methods, pitfalls, and challenges. Int J Radiat Oncol Biol Phys 2018;102:1117-42.
14. Gillies RJ, Kinahan PE, Hricak H. Radiomics: Images are more than pictures. They are data. Radiology 2016;278:563-77.
15. Rahmim A, Huang P, Shenkov N, Fotouhi S, Davoodi-Bojd E, Lu L, et al. Improved prediction of outcome in Parkinson's disease using radiomics analysis of longitudinal DAT SPECT images. Neuroimage Clin 2017;16:539-44.
16. Shiiba T, Arimura Y, Nagano M, Takahashi T, Takaki A. Improvement of classification performance of Parkinson's disease using shape features for machine learning on dopamine transporter single photon emission computed tomography. PLOS ONE 2020;15:e0228289.
17. Hajianfar G, Shiri I, Maleki H, Oveisi N, Haghparast A, Abdollahi H, et al. Noninvasive O6 methylguanine-DNA methyltransferase status prediction in glioblastoma multiforme cancer using magnetic resonance imaging radiomics features: Univariate and multivariate radiogenomics analysis. World Neurosurg 2019;132:e140-61.
18. Ashrafinia S, Dalaie P, Yan R, Ghazi P, Marcus C, Taghipour M, et al. Radiomics analysis of clinical myocardial perfusion SPECT to predict coronary artery calcification. J Nucl Med 2018;59:512.
19. Ashrafinia S, Dalaie P, Yan R, Huang P, Pomper M, Schindler T, et al. Application of texture and radiomics analysis to clinical myocardial perfusion SPECT imaging [Abstract]. J Nucl Med 2018;59:94.
20. Kolossváry M, Karády J, Szilveszter B, Kitslaar P, Hoffmann U, Merkely B, et al. Radiomic features are superior to conventional quantitative computed tomographic metrics to identify coronary plaques with napkin-ring sign. Circ Cardiovasc Imaging 2017;10:e006843.
21. Neisius U, El-Rewaidy H, Nakamori S, Rodriguez J, Manning WJ, Nezafat R. Radiomic analysis of myocardial native T1 imaging discriminates between hypertensive heart disease and hypertrophic cardiomyopathy. JACC Cardiovasc Imaging 2019;12:1946-54.
22. Ashrafinia S. Quantitative nuclear medicine imaging using advanced image reconstruction and radiomics. Baltimore: Johns Hopkins University; 2019.
23. Ashrafinia S, Dalaie P, Sadaghiani MS, Schindler T, Pomper M, Rahmim A. Standardized Radiomics of clinical myocardial perfusion stress SPECT images to determine coronary artery calcification score. Eur J Nucl Med Mol Imaging 2019;46:S17-8.
24. Motwani M. Hiding beyond plain sight: Textural analysis of positron emission tomography to identify high-risk plaques in carotid atherosclerosis. J Nucl Cardiol 2019. https://doi.org/10.1007/s12350-019-01981-9.
25. Hatt M, Tixier F, Pierce L, Kinahan PE, Le Rest CC, Visvikis D. Characterization of PET/CT images using texture analysis: the past, the present… any future? Eur J Nucl Med Mol Imaging 2017;44:151-65.
26. Zwanenburg A, Leger S, Vallières M, Löck S. Image biomarker standardisation initiative. arXiv preprint arXiv:161207003; 2016.

27. Traverso A, Wee L, Dekker A, Gillies R. Repeatability and reproducibility of radiomic features: A systematic review. Int J Radiat Oncol Biol Phys 2018;102:1143-58.
28. Kalendralis P, Traverso A, Shi Z, Zhovannik I, Monshouwer R, Starmans MPA, et al. Multicenter CT phantoms public dataset for radiomics reproducibility tests. Med Phys 2019;46:1512-8.
29. Pfaehler E, Beukinga RJ, de Jong JR, Slart R, Slump CH, Dierckx R, et al. Repeatability of (18) F-FDG PET radiomic features: A phantom study to explore sensitivity to image reconstruction settings, noise, and delineation method. Med Phys 2019;46:665-78.
30. Shiri I, Rahmim A, Ghaffarian P, Geramifar P, Abdollahi H, Bitarafan-Rajabi A. The impact of image reconstruction settings on 18F-FDG PET radiomic features: Multi-scanner phantom and patient studies. Eur Radiol 2017;27:4498-509.
31. Raunig DL, McShane LM, Pennello G, Gatsonis C, Carson PL, Voyvodic JT, et al. Quantitative imaging biomarkers: A review of statistical methods for technical performance assessment. Stat Methods Med Res 2015;24:27-67.
32. Fedorov A, Beichel R, Kalpathy-Cramer J, Finet J, Fillion-Robin J-C, Pujol S, et al. 3D Slicer as an image computing platform for the Quantitative Imaging Network. Magn Reson Imaging 2012;30:1323-41.
33. Van Griethuysen JJ, Fedorov A, Parmar C, Hosny A, Aucoin N, Narayan V, et al. Computational radiomics system to decode the radiographic phenotype. Cancer Res 2017;77:e104-7.
34. Yan J, Chu-Shern JL, Loi HY, Khor LK, Sinha AK, Quek ST, et al. Impact of image reconstruction settings on texture features in 18F-FDG PET. J Nucl Med 2015;56:1667-73.
35. Buvat I, Orlhac F. The dark side of radiomics: On the paramount importance of publishing negative results. J Nucl Med 2019;60:1543-4.
36. Kolossváry M, Karády J, Kikuchi Y, Ivanov A, Schlett CL, Lu MT, et al. Radiomics versus visual and histogram-based assessment to identify atheromatous lesions at coronary CT angiography: An ex vivo study. Radiology 2019;293:89-96.
37. Arad Y, Goodman KJ, Roth M, Newstein D, Guerci AD. Coronary calcification, coronary disease risk factors, C-reactive protein, and atherosclerotic cardiovascular disease events: The St. Francis Heart Study. J Am Coll Cardiol 2005;46:158-65.
38. Haberl R, Becker A, Leber A, Knez A, Becker C, Lang C, et al. Correlation of coronary calcification and angiographically documented stenoses in patients with suspected coronary artery disease: Results of 1,764 patients. J Am Coll Cardiol 2001;37:451-7.
39. Berman DS, Wong ND, Gransar H, Miranda-Peats R, Dahlbeck J, Hayes SW, et al. Relationship between stress-induced myocardial ischemia and atherosclerosis measured by coronary calcium tomography. J Am Coll Cardiol 2004;44:923-30.
40. He Z-X, Hedrick TD, Pratt CM, Verani MS, Aquino V, Roberts R, et al. Severity of coronary artery calcification by electron beam computed tomography predicts silent myocardial ischemia. Circulation 2000;101:244-51.
41. Abdollahi H, Shiri I, Heydari M. Medical imaging technologists in radiomics era: An alice in wonderland problem. Iran J Public Health. 2019;48:184.